Preparation and Acid–Base Properties of a Protonated Titanate with the Lepidocrocite-like Layer Structure

Takayoshi Sasaki,* Mamoru Watanabe, Yuichi Michiue, Yu Komatsu, Fujio Izumi, and Satoshi Takenouchi

National Institute for Research in Inorganic Materials, 1-1 Namiki, Tsukuba, Ibaraki 305, Japan

Received January 4, 1995. Revised Manuscript Received March 9, 1995[⊗]

A layered solid acid, $H_xTi_{2-x/4}\square_{x/4}O_4 \cdot H_2O$ (□: vacancy, $x \sim 0.7$), has been prepared by acid exchange of a cesium titanate, $Cs_xTi_{2-x/4}\square_{x/4}O_4$. The body-centered orthorhombic structure comprises host layers of lepidocrocite-type and interlayer H_2O molecules, 70% of which are protonated to be H_3O^+. The material undergoes ion-exchange and intercalation reactions at ambient temperature. Alkali metal ions were taken up continuously via solid solution up to ~70% substitution of exchangeable protons, forming monolayer hydrates with the interlayer separation of ~9 Å. The reaction beyond the loading proceeded only for Na and Li ions, which yielded bilayer hydrates. The distinctive threshold loading of 70% dominating two defined hydrate structures corresponds to the half-occupation of interlayer pseudocubic cavities by guest cations. Rietveld refinements for the cation-loaded phases formed at the threshold supported the monolayer arrangement in which cations and water molecules alternate.

Introduction

A number of layered materials have been synthesized in the ternary or quaternary system of alkali metal, titanium, and/or niobium and oxygen: titanates[1–5] ($K_2Ti_2O_5$, $Na_2Ti_3O_7$, $K_2Ti_4O_9$, $Cs_2Ti_5O_{11}$, and $Cs_xTi_{2-x/4}\square_{x/4}O_4$ where □ expresses vacancy), niobates[6,7] (KNb_3O_8 and $K_4Nb_6O_{17}$), and titanoniobates[8–10] ($KTiNbO_5$, $CsTi_2NbO_7$, KTi_3NbO_9, and $K_3Ti_5NbO_{14}$). One of the most recent and intriguing topics concerning these layered compounds is their prominent photocatalytic activities.[11,12] UV–visible light irradiation generates electrons and positive holes in the host layers because of their semiconductive nature, which exhibit highly reductive and oxidative power. It has been reported,[11] for example, that $K_4Nb_6O_{17}$ photodecomposes very efficiently interlayer H_2O molecules to H_2 and O_2 gas in a stoichiometric ratio. These photocatalytic reactions take place in interlayer galleries and consequently should be strongly influenced by their chemical and structural environments. Thus, to optimize the photocatalytic activities, it is of fundamental importance to get information on the nature of interlayer spaces.

The interlayer chemistry of these materials has been studied extensively. Most of these compounds can be converted into protonated forms preserving their layer structures.[13–17] Resulting protonic oxides exhibit distinctive solid acidity, incorporating a wide variety of guests such as cations and organic bases, from small to large in size, into their interlayer spaces.[14b,15,18–24] This property invites various practical potentials such as ion exchangers,[25] separations,[26] preparation of microporous

[⊗] Abstract published in *Advance ACS Abstracts,* April 15, 1995.

(1) Andersson, S.; Wadsley, A. D. *Acta Chem. Scand.* **1961**, *15*, 663.
(2) Andersson, S.; Wadsley, A. D. *Acta Crystallogr.* **1961**, *14*, 1245.
(3) (a) Verbaere, A.; Tournoux, M. *Bull. Soc. Chim. Fr.* **1973**, *4*, 1237. (b) Dion, M.; Piffard, Y.; Tournoux, M. *J. Inorg. Nucl. Chem.* **1978**, *40*, 917.
(4) (a) Grey, I. E.; Madsen, I. C.; Watts, J. A.; Bursill, L. A.; Kwiatkowska, J. *J. Solid State Chem.* **1985**, *58*, 350. (b) Kwiatkowska, J.; Grey, I. E.; Madsen, I. C.; Bursill, L. A. *Acta Crystallogr.* **1987**, *B43*, 258.
(5) (a) Hervieu, M.; Raveau, B. *Rev. Chim. Miner.* **1981**, *18*, 642. (b) Grey, I. E.; Madsen, I. C.; Watts, J. A. *J. Solid State Chem.* **1987**, *66*, 7.
(6) Gasperin, M. *Acta Crystallogr.* **1982**, *B38*, 2024.
(7) (a) Nassau, K.; Shiever, J. W.; Bernstein, J. L. *J. Electrochem. Soc.* **1969**, *116*, 348. (b) Gasperin, M.; Bihan, M. T. Le *J. Solid State Chem.* **1980**, *33*, 89.
(8) Wadsley, A. D. *Acta Crystallogr.* **1964**, *17*, 623.
(9) Hervieu, M.; Raveau, B. *J. Solid State Chem.* **1980**, *32*, 161.
(10) Hervieu, M.; Rebbah, H.; Desgardin, G.; Raveau, B. *J. Solid State Chem.* **1980**, *35*, 200.
(11) (a) Domen, K.; Kudo, A.; Shibata, M.; Tanaka, A.; Maruya, K.; Onishi, T. *J. Chem. Soc., Chem. Commun.* **1986**, 1706. (b) Kudo, A.; Sayama, K.; Tanaka, A.; Asakura, K.; Domen, K.; Maruya, K.; Onishi, T. *J. Catal.* **1989**, *120*, 337. (c) Kudo, A.; Tanaka, A.; Domen, K.; Maruya, K.; Aika, K.; Onishi, T. *J. Catal.* **1989**, *111*, 67. (d) Sayama, K.; Tanaka, A.; Domen, K.; Maruya, K.; Onishi, T. *J. Phys. Chem.* **1991**, *95*, 1345.
(12) (a) Kim, Y. I.; Salim, S.; Huq, M. J.; Mallouk, T. E. *J. Am. Chem. Soc.* **1991**, *113*, 9561. (b) Kim, Y. I.; Atherton, S. J.; Brigham, E. S.; Mallouk, T. E. *J. Phys. Chem.* **1993**, *97*, 11802.
(13) (a) Izawa, H.; Kikkawa, S.; Koizumi, M. *J. Phys. Chem.* **1982**, *86*, 5023. (b) Feist, T. P.; Mocarski, S. J.; Davies, P. K.; Jacobson, A. J.; Lewandowski, J. T. *Solid State Ionics* **1988**, *28–30*, 1338. (c) Feist, T. P.; Davies, P. K. *J. Solid State Chem.* **1992**, *101*, 275.
(14) (a) Marchand, R.; Brohan, L.; Tournoux, M. *Mater. Res. Bull.* **1980**, *15*, 1129. (b) Sasaki, T.; Watanabe, M.; Komatsu, Y.; Fujiki, Y. *Inorg. Chem.* **1985**, *24*, 2265.
(15) Sasaki, T.; Komatsu, Y.; Fujiki, Y. *Chem. Mater.* **1992**, *4*, 894.
(16) Nedjar, R.; Borel, M. M.; Raveau, B. *Mater. Res. Bull.* **1985**, *20*, 1291.
(17) Rebbah, H.; Desgardin, G.; Raveau, B. *Mater. Res. Bull.* **1979**, *14*, 1125.
(18) Izawa, H.; Kikkawa, S.; Koizumi, M. *Polyhedron* **1983**, *2*, 741.
(19) (a) Clément, P.; Marchand, R. *C. R. Acad. Sci. Paris, Ser. II* **1983**, *296*, 1161. (b) Sasaki, T.; Watanabe, M.; Komatsu, Y.; Fujiki, Y. *Bull. Chem. Soc. Jpn.* **1985**, *58*, 3500. (c) Sasaki, T.; Komatsu, Y.; Fujiki, Y. *Mater. Res. Bull.* **1987**, *22*, 1321. (d) Miyata, H.; Sugahara, Y.; Kuroda, K.; Kato, C. *J. Chem. Soc., Faraday Trans. 1* **1988**, *84*, 2677. (e) Sasaki, T.; Komatsu, Y.; Fujiki, Y. *Inorg. Chem.* **1989**, *28*, 2776.
(20) (a) Nedjar, R.; Borel, M. M.; Raveau, B. *Z. Anorg. Allg. Chem.* **1986**, *540*, 198. (b) Nedjar, R.; Borel, M. M.; Raveau, B. *J. Solid State Chem.* **1987**, *71*, 451.
(21) Kinomura, N.; Kumada, N.; Muto, F. *J. Chem. Soc., Dalton Trans.* **1985**, 2349.

0897-4756/95/2807-1001$09.00/0

materials,[27] and solidification/immobilization of radioactive nuclides.[28]

The Cs titanate, $Cs_xTi_{2-x/4}\square_{x/4}O_4$, possesses a layer structure which is related to that of lepidocrocite FeO(OH).[29] The compound is characterized by its relatively simple architecture and the low negative charge density of the host layer in comparison with the other titanates, niobates, and titanoniobates above.[30] Although these features make us anticipate high intercalation reactivity, there has been few reports centering on such a subject. Several isomorphous compounds have been synthesized by substituting Ti with lower valent cations, e.g., Mg, Fe.[31] England et al. have studied ion-exchange reactions in $Cs_xTi_{2-x/2}Mg_{x/2}O_4$ and demonstrated that Cs ions can be exchanged spontaneously for other cations in molten and aqueous media.[32] Unfortunately, they did not present the data on solid acidity of the protonated form. It is also to be pointed out that a different charge compensation scheme via Ti site vacancies instead of Mg substitution may show a significant deviation between these two compositions.

The present study describes conversion of lepidocrocite-related titanate, $Cs_xTi_{2-x/4}\square_{x/4}O_4$, into a protonated form and its acid–base intercalation behavior. Intercalated products are examined from a structural aspect to clarify how guest species are accommodated, by which deeper interpretation on the reaction mechanism is achieved.

Experimental Section

Reagents and Materials. The reagents such as TiO_2 and Cs_2CO_3 of 99.99% purity and the other chemicals of reagent grade were obtained from commercial sources and used as supplied.

The Cs titanate $Cs_xTi_{2-x/4}\square_{x/4}O_4$ was synthesized by a conventional solid-state procedure akin to that reported by Grey et al.[5b] An intimate mixture of Cs_2CO_3 and TiO_2 was placed in a Pt crucible with a tight lid and was heated at 800 °C for 1 h to be decarbonated. The mixture was ground and then allowed to 2 cycles of heating (800 °C, 20 h) with grinding at the interval. The calcined products were white, microcrystalline powders of micrometer dimension. The chemical analyses indicated negligible evaporative loss of Cs during the firing. The powder X-ray diffraction (XRD) demonstrated that a single phase of lepidocrocite-related titanate was obtained where the molar ratio of Cs_2CO_3/TiO_2 was $^1/_{5.5}-^1/_{5.1}$. This indicates that x in $Cs_xTi_{2-x/4}\square_{x/4}O_4$ spans from 0.67 to 0.73. The material of mean stoichiometry, namely, $x = 0.70$, was used in the experiments below.

An acid exchange form was derived from the Cs titanate, $Cs_xTi_{2-x/4}\square_{x/4}O_4$, by leaching it in an aqueous HCl solution at ambient temperature. The HCl concentration was 1 mol dm^{-3}, and the solution-to-solid ratio was 100 cm^3g^{-1}. The leaching was repeated by replacing the solution with a fresh one every 24 h. The material was rinsed with copious water to remove excess HCl and then dried over a saturated NaCl solution (relative humidity 70%).

Equilibrations. Distribution coefficients, K_d, were measured as a function of pH by shaking 0.1 g of $H_xTi_{2-x/4}\square_{x/4}O_4\cdot H_2O$ with 10 cm^3 of aqueous solutions containing alkali metal chlorides (concentration 1×10^{-3} mol dm^{-3}) at 25 ± 0.5 °C for 7 days. The pH value was controlled by adding an appropriate amount of HCl solutions. The equilibrated solutions were analyzed for their residual cation concentration as well as pH value, the data from which K_d values were calculated by the following equation:

$$K_d = (\text{mol of metal ion/g of solid})/(\text{mol of metal ions/cm}^3\text{ of solution}) \quad (1)$$

The amount of cations in the solid was estimated by deducting concentrations of equilibrated solutions from the initial value.

The titration was carried out in a batchwise procedure[14b,15] by equilibrating $H_xTi_{2-x/4}\square_{x/4}O_4\cdot H_2O$ with alkali metal chloride/hydroxide solutions at 25 ± 0.5 °C. The solution-to-solid ratio was 100 cm^3 g^{-1}, and the ionic strength of the solutions was 0.1. After equilibrium was attained, the pH values and cation concentrations of the aqueous solutions were measured in a manner similar to the case in the distribution coefficient determination. Solid phases, separated from the solutions and conditioned at a relative humidity of 70%, were examined by means of powder XRD, TG-DTA, and chemical analysis.

Chemical Analysis. A weighed amount (~100 mg) of the titanate, either protonated or alkali metal ion loaded, was dissolved with a mixed acid solution (10 cm^3 of 1/1 H_2SO_4 + 2.5 cm^3 concentrated HF) by heating it at 160 °C in a Teflon-lined vessel. The liquid was transferred to a Pt pan and was evaporated to dryness to remove excess HF. A solid residue was dissolved with a 1/100 H_2SO_4 solution. The alkali-metal ions and Ti in the solution were determined by atomic absorption spectroscopy and gravimetry using cupferron as a precipitant, respectively. The water content was estimated from the weight loss at 800 °C.

Instrumentation. The powder XRD data were acquired by a Rigaku RAD-2B diffractometer with graphite-monochromatized Cu Kα radiation (λ = 1.5405 Å). Lattice parameters were refined by a least-squares method.[33] Rietveld analyses were carried out using the program RIETAN[34] on intensity data collected in a step-scan mode (step interval 0.03° in 2θ) over an angular range 19–100°.

FT-IR spectra were recorded using a Bio-Rad FTS-45RD spectrometer (resolution 2 cm^{-1}). Simultaneous DTA/TGA measurements were performed using a Rigaku TAS 200 thermalanalyzer at a heating rate of 10 °C min^{-1}. A Hitachi 180-80 atomic absorption spectrophotometer was employed to determine alkali-metal ion contents in aqueous phases.

Results and Discussion

Protonation of the Titanate. The removal of interlayer Cs ions, which is formulated as below,

(22) (a) Rebbah, H.; Borel, M. M.; Raveau, B. *Mater. Res. Bull.* **1980**, *15*, 317. (b) Grandin, A.; Borel, M. M.; Raveau, B. *J. Solid State Chem.* **1985**, *60*, 366.
(23) Rebbah, H.; Hervieu, M.; Raveau, B. *Ann. Chim.* **1981**, *6*, 653.
(24) Grandin, A.; Borel, M. M.; Raveau, B. *Rev. Chim. Miner.* **1981**, *18*, 322.
(25) (a) Izawa, H.; Kikkawa, S.; Koizumi, M. *J. Solid State Chem.* **1985**, *60*, 264. (b) Izawa, H.; Kikkawa, S.; Koizumi, M. *J. Solid State Chem.* **1987**, *69*, 336.
(26) (a) Komatsu, Y.; Fujiki, Y.; Sasaki, T. *Bunseki Kagaku* **1983**, *32*, 33. (b) Sasaki, T.; Komatsu, Y.; Fujiki, Y. *Sep. Sci. Technol.* **1983**, *18*, 49. (c) Sasaki, T.; Komatsu, Y.; Fujiki, Y. *J. Radioanal. Nucl. Chem.* **1987**, *107*, 111. (d) Komatsu, Y.; Fujiki, Y.; Sasaki, T. *Solvent Extr. Ion Exch.* **1993**, *11*, 159.
(27) (a) Cheng, S.; Wang, T. *Inorg. Chem.* **1989**, *28*, 1283. (b) Anderson, M. W.; Klinowski, J. *Inorg. Chem.* **1990**, 29, 3260. (c) Landis, M. E.; Aufdembrink, B. A.; Chu, P.; Johnson, I. D.; Kirker, G. W.; Rubin, M. K. *J. Am. Chem. Soc.* **1991**, *113*, 3189. (d) Sylvester, P.; Cahill, R.; Clearfield, A. *Chem. Mater.* **1994**, *6*, 1890.
(28) (a) Fujiki, Y.; Komatsu, Y.; Sasaki, T.; Ohta, N. *Nippon Kagaku Kaishi* **1981**, 1656. (b) Sasaki, T.; Komatsu, Y.; Fujiki, Y. *Chem. Lett.* **1981**, 957.
(29) Ewing, T. J. *J. Chem. Phys.* **1935**, *3*, 420.
(30) Sasaki, T.; Komatsu, Y.; Fujiki, Y. *J. Chem. Soc., Chem. Commun.* **1991**, 894.
(31) (a) Reid, A. F.; Mumme, W. G.; Wadsley, A. D. *Acta Crystallogr.* **1968**, *B24*, 1228. (b) Groult, D.; Mercy, C.; Raveau, B. *J. Solid State Chem.* **1980**, *32*, 289.
(32) England, W. A.; Birkett, J. E.; Goodenough, J. B.; Wiseman, P. J. *J. Solid State Chem.* **1983**, *49*, 300.
(33) Appleman, D. E.; Evans, H. T., Jr. Report No. PB216188, U.S. Department of Commerce, National Technical Information Service: Springfield, VA, 1973.
(34) Izumi, F. *The Rietveld Method*; Young, R. A., Ed.; Oxford University Press: Oxford, 1993.

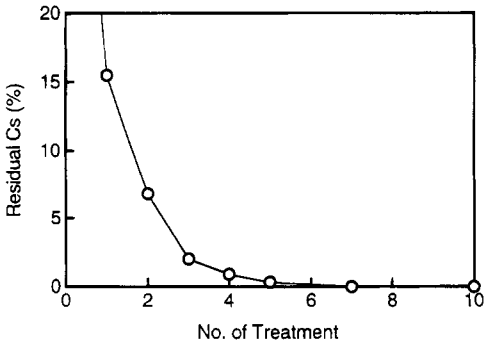

Figure 1. Cs ion extraction by acid leaching.

Table 1. Lattice Parameters before and after the Acid Treatment

compound	a (Å)	b (Å)	c (Å)
$Cs_xTi_{2-x/4}\square_{x/4}O_4$	3.837(1)	17.198(3)	2.960(1)
$H_xTi_{2-x/4}\square_{x/4}O_4{\cdot}H_2O$	3.783(2)	18.735(8)	2.978(2)

proceeded by repeating the acid leaching (see Figure 1):

$$Cs_xTi_{2-x/4}\square_{x/4}O_4(s) + xH^+(aq) + H_2O(aq) \rightarrow H_xTi_{2-x/4}\square_{x/4}O_4{\cdot}H_2O(s) + xCs^+(aq) \quad (2)$$

The water content was determined to be approximately one per chemical formula from the gross weight loss of ~14% at 800 °C. Table 1 lists the lattice constants for the material produced after three cycles of the acid treatment, which achieved a substantially full (~98%) removal of Cs ions. The body-centered symmetry as well as the unit cell dimensions gives the crystal structure shown in Figure 2. Two noticeable structural changes took place on acid exchange; the increment of the interlayer spacing (d_{020}) from 8.6 to 9.4 Å and incorporation of one H_2O molecule in every pseudocubic site in the interlayer region. Note that only 70% of the sites are occupied by Cs ions in the parent titanate.

The complete extraction of Cs ions to a negligible level resulted in introduction of structural disorder, degrading the body-centered cell. The diffraction lines of *hk*0 and *hkl* became broad and finally smeared out. The other reflections remained virtually unchanged. The lattice parameters obtained from particular diffraction lines were hardly different from those in Table 1. This disorder is interpreted in terms of random gliding of the host layers along the *a* axis. This may be due to the loss of Cs ions which play a role in pinning adjacent layers. A regular layer sequence was restored reversibly upon intercalation of appropriate guests.

The FT-IR spectrum for $H_xTi_{2-x/4}\square_{x/4}O_4{\cdot}H_2O$ (Figure 3) had two prominent absorption bands at 3400 and 1630 cm^{-1}, which are assignable as stretching and bending vibrations of H_2O (H_3O^+), respectively.[35] The IR data for the other types of layered protonic titanates, $H_2Ti_3O_7$, $H_2Ti_4O_9{\cdot}1.2H_2O$, and $H_2Ti_5O_{11}{\cdot}3H_2O$, exhibited a distinctive absorption at 970 cm^{-1} besides the two bands above.[13-15] This is indicative of the presence of a hydroxyl group as well as interlayer H_2O (H_3O^+).[35] The host layers in $H_2Ti_3O_7$, $H_2Ti_4O_9{\cdot}1.2H_2O$, and $H_2Ti_5O_{11}{\cdot}3H_2O$ are stepped at a regular length, every three, four, and five octahedra, respectively (see Figure 4).[2-4] Nonshared oxygen atoms at the stepping corner

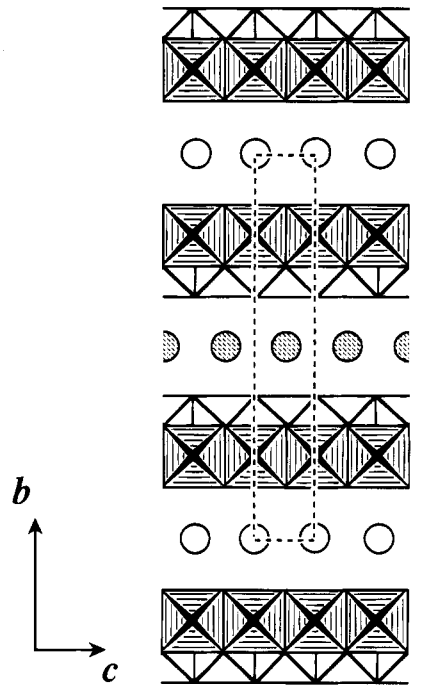

Figure 2. Polyhedral representation of the crystal structure for $H_xTi_{2-x/4}\square_{x/4}O_4{\cdot}H_2O$ viewed down along the *a* axis. Open and stippled circles represent H_2O (or H_3O^+) at $x = 0$ and $1/2$, respectively. Broken lines encircle the body-centered unit cell.

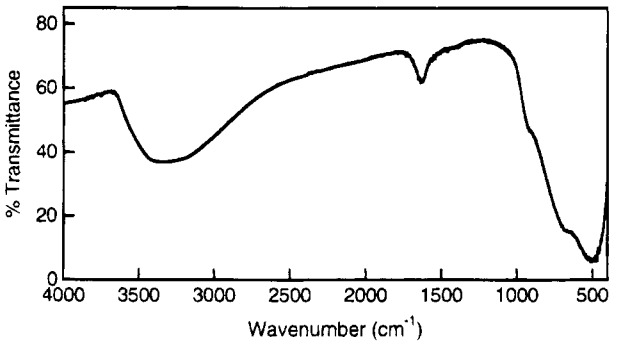

Figure 3. FT-IR data for $H_xTi_{2-x/4}\square_{x/4}O_4{\cdot}H_2O$.

are hydroxylated on protonation because of its high basicity. This has been verified by structure refinements[13c] and theoretical calculations.[36] In contrast, the layer in $H_xTi_{2-x/4}\square_{x/4}O_4{\cdot}H_2O$ is not stepped but rather straight without oxygen atoms to be protonated. The material accommodates exchangeable protons in the form of H_3O^+, not hydroxyls.

The protonic titanate, $H_xTi_{2-x/4}\square_{x/4}O_4{\cdot}H_2O$, underwent dehydration in overlapping two steps, 40–140 and 140–450 °C (see Figure 5), the weight loss of which amounted to approximately 10 and 4%, respectively. The XRD data on an intermediate at 140 °C indicated that the layer structure was maintained, although its crystallinity was degraded. The contracted interlayer separation of 6.6 Å is close to that of lepidocrocite FeO(OH) which does not contain interlayer guests.[29] The weight loss data as well as the structural evidence suggest that the dehydration in step I is ascribed to evaporation of interlayer H_2O molecules, producing $H_xTi_{2-x/4}\square_{x/4}O_4$. The subsequent heating in step II collapsed the layer structure and resulted in an amorphous material. Further heating promoted to crystallize anatase. The

(35) Ryskin, Y. I. *The Infrared Spectra of Minerals*; Farmer, V. C., Ed.; Mineralogical Society: London, 1974.

(36) Dronskowski, R. *J. Am. Chem. Soc.* **1992**, *114*, 7230.

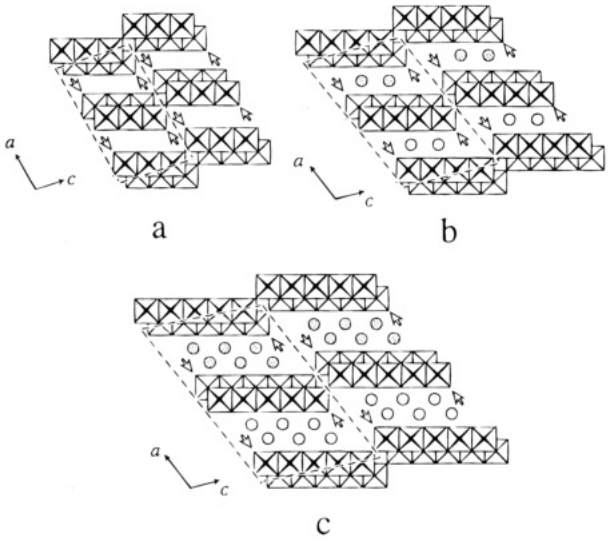

Figure 4. Idealized crystal structures of protonic layered titanates: (a) $H_2Ti_3O_7$, (b) $H_2Ti_4O_9 \cdot 1.2H_2O$, (c) $H_2Ti_5O_{11} \cdot 3H_2O$. Broken lines encircle *C*-base centered monoclinic unit cells. Circles and arrows denote H_2O (H_3O^+) and position of hydroxylated proton, respectively. In $H_2Ti_3O_7$, another mole of protons besides indicated ones (terminal hydroxyls) is distributed over surface oxygen atoms.[13c]

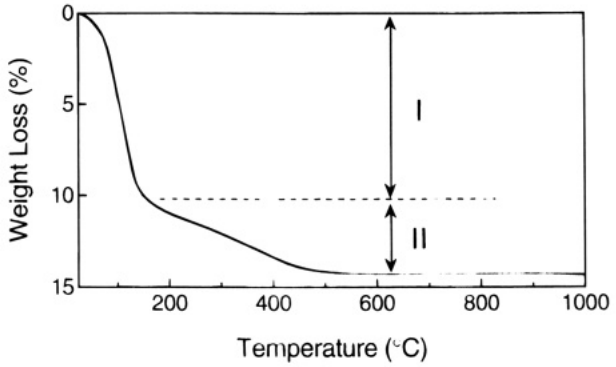

Figure 5. Thermogravimetric curve for $H_xTi_{2-x/4}\square_{x/4}O_4 \cdot H_2O$.

dehydration process may be summarized as follows.

$$H_xTi_{2-x/4}\square_{x/4}O_4 \cdot H_2O \xrightarrow{140\ ^\circ C} H_xTi_{2-x/4}\square_{x/4}O_4 \xrightarrow{450\ ^\circ C} TiO_2(\text{anatase}) \quad (3)$$

Direct crystallization of anatase is contrasting to the dehydration behaviors of the other types of protonic titanates, $H_2Ti_3O_7$, $H_2Ti_4O_9 \cdot 1.2H_2O$, and $H_2Ti_5O_{11} \cdot 3H_2O$. It has been reported[13b,c,14a,15] that upon complete dehydration the materials evolve a novel polymorph of titanium dioxide, TiO_2(B), which is metastable, being transformed into anatase at higher temperatures. This difference suggests that the stepping host layers with hydroxyls at the corners and dehydrating condensation between them may be a key to construct the TiO_2(B) structure.

Acid–Base Intercalation Reactivity. Figure 6 illustrates sorption characteristics of alkali metal ions at a microquantity level. The logarithms of distribution coefficient were correlated by a straight line with the pH values. The slope of ~1, being equal to the charge of the cations, is accounted for by one-to-one exchange between protons in $H_xTi_{2-x/4}\square_{x/4}O_4 \cdot H_2O$ and alkali metal ions in aqueous solutions.[37]

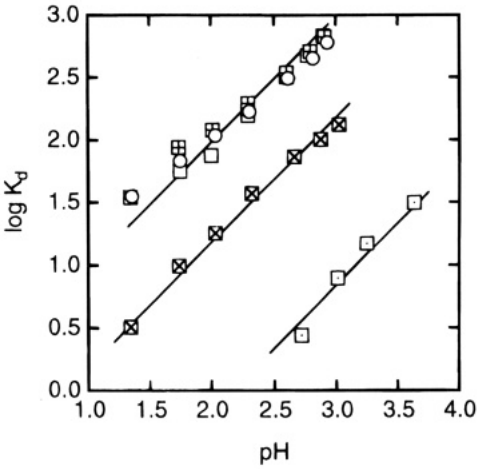

Figure 6. Distribution coefficient as a function of pH. (□) Cs, (box with plus sign) Rb, (○) K, (box with times sign) Na, (⊡) Li.

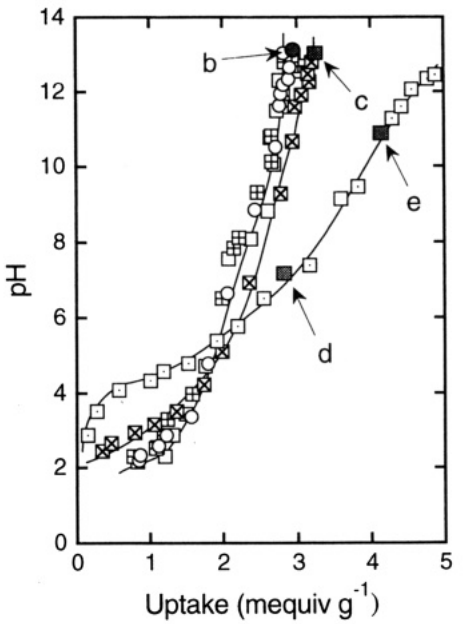

Figure 7. Titration curves. (□) Cs, (box with plus sign) Rb, (○) K, (box with times sign) Na, (⊡) Li. Powder X-ray data for titrated products indicated by b–e are shown in Figure 8.

The titration curves are shown in Figure 7. The cation uptake increased smoothly with the pH value, suggesting unifunctional acidity of the material. The cations heavier than K exhibited very similar behavior. The saturated capacity for these cations corresponds to ~70% consumption of exchangeable protons.[38] On the other hand, ~80% substitution was the case for Na ion and overloading beyond the theoretical limit was found for Li ion. The reason for the overloading is unknown.

The alkali metal ion selectivity was Cs ~ Rb ~ K > Na > Li at an early stage of the exchange, which is in accord with the order from distribution study (Figure 6). This sequence has been widely observed in a variety of ion exchangers[39] and is explained in terms of hydration energy of the cations. The selectivity order was

(37) (a) Ahrland, S., Albertsson, J. *Acta Chem. Scand.* **1964**, *18*, 1861. (b) Tsuji, M.; Abe, M. *Solvent Extr. Ion Exch.* **1984**, *2*, 253.

(38) 4.12 mequiv g^{-1}, a theoretical value based on the composition $H_xTi_{2-x/4}\square_{x/4}O_4 \cdot H_2O$ where $x = 0.7$.

(39) Clearfield, A. *Inorganic Ion Exchange Materials*; CRC Press: Boca Raton, FL, 1982.

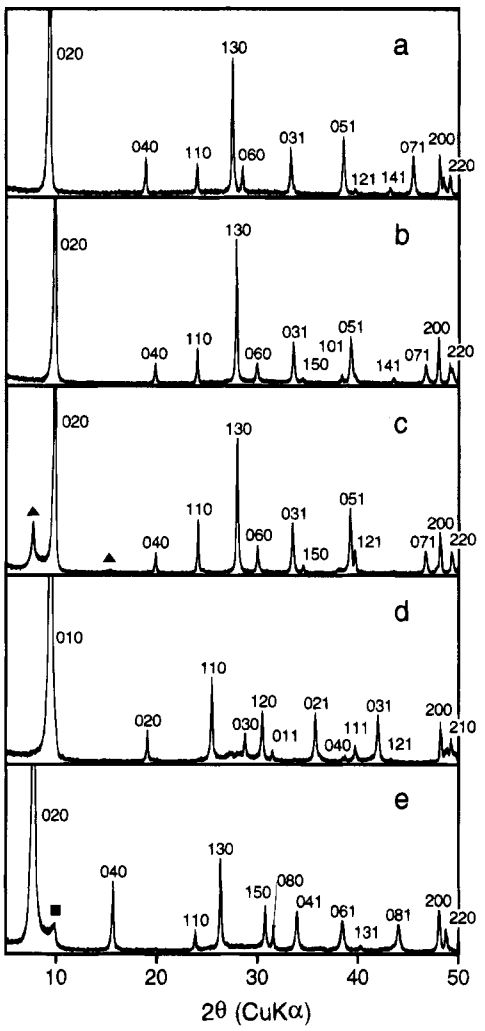

Figure 8. Powder X-ray diffraction patterns for cation-loaded phases. (a) $H_xTi_{2-x/4}\square_{x/4}O_4 \cdot H_2O$, (b) K phase (70% loading), (c) Na phase (80%), (d) Li phase (70%), and (e) Li phase (95%). Triangles in (c) indicate the swollen phase with interlayer spacing of 11.5 Å. A square in (e) denotes the persisting 70% phase shown in (d).

eventually inverted in a high loading region, which may be attributable to the size effect.

The material exhibited Brønsted acidity to take up alkyl amines and pyridine. It is noteworthy that $H_xTi_{2-x/4}\square_{x/4}O_4 \cdot H_2O$ is a stronger solid acid than the other types of protonic layered titanates, $H_2Ti_3O_7$, $H_2Ti_4O_9 \cdot 1.2H_2O$, and $H_2Ti_5O_{11} \cdot 3H_2O$, which do not intercalate pyridine.[19a,40] The details will be described elsewhere.

Structural Changes. Continuous solid solution was formed in the entire range of K, Rb, and Cs ion incorporation processes, preserving a body-centered orthorhombic lattice. The interlayer distance shrank upon cation intercalation, being 9.0 (Figure 8b), 8.6, and 8.8 Å for final products (70% loading) of K, Rb, and Cs ions, respectively. The Na ion exchange proceeded in a similar manner up to 70% conversion, producing an 8.9 Å phase of body-centered symmetry. A further reaction evolved a highly swollen phase as indicated by triangles in Figure 8c. On the other hand, Li ion uptake was accompanied by changes in lattice type. The body-centered orthorhombic structure for $H_xTi_{2-x/4}\square_{x/4}O_4 \cdot H_2O$ changed into a primitive lattice up to 70% substitution (Figure 8d), which was subsequently transformed into a *C*-base-centered phase with a largely expanded interlayer spacing of 11.3 Å (Figure 8e). The structural changes induced by the cation incorporation are summarized in Figure 9. The chemical composition and crystallographic data for the evolved phases are tabulated in Table 2. The lattice parameters give an evidence that the host layer of lepidocrocite-type was retained throughout. The lattice type changes observed in Li ion incorporation can be understood as modification of relative configuration of the host layers. Neighboring host layers are displaced with respect to one another by $(a + c)/2$ in the loading range of 0−70% and then $c/2$ for further exchange.

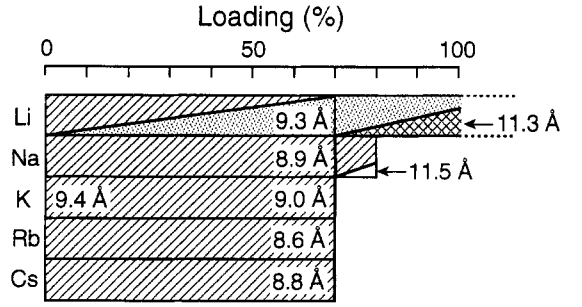

Figure 9. Alkali-metal ion incorporation processes. Areas with hatched, stippled, and cross-hatched patterns express body-centered, primitive, and *C*-base-centered phases, respectively.

Table 2. Unit-Cell Dimensions for the Cation-Loaded Phases

guest ion	loading (%)	n_{H_2O}[a]	lattice type	*a* (Å)	*b* (Å)	*c* (Å)
Li	70	1.0	*P*	3.7742(4)	9.317(1)	2.9829(4)
	100	1.7	*C*	3.7864(6)	22.642(3)	2.9876(4)
Na	70	0.9	*I*	3.7825(3)	17.901(2)	2.9889(2)
K	70	0.7	*I*	3.7896(8)	17.908(4)	2.9854(6)
Rb	70	0.6	*I*	3.796(1)	17.232(8)	2.9702(7)
Cs	70	0.5	*I*	3.8019(2)	17.720(1)	2.9680(2)

[a] *n* in $A_yH_{x-y}Ti_{2-x/4}\square_{x/4}O_4 \cdot nH_2O$, where *A* denotes alkali metal ions.

Interpretation of the Threshold Loading. The alkali metal ion intercalation processes, summarized in Figure 9, demonstrate a threshold conversion of 70% where two distinguishing changes took place: (i) cessation of exchange reaction for K, Rb, and Cs ions and (ii) abrupt expansion of the lattice for Li and Na ions. The phases formed below the threshold, having the interlayer spacing of ~9 Å, are due to monolayer arrangements of cations and H_2O molecules in the galleries (Figure 10a). The water content of the solid, n_{H_2O} in Table 2, tended to decrease in this conversion range, which suggests that ingoing cations replace interlayer H_3O^+ ions. On the other hand, the phases occurred beyond the threshold are likely to have a bilayer water/cation cluster (Figure 10b), which is evidenced by a marked increase in water contents as well as interlayer spacing. The expansion of ~2.5 Å is in harmony with the thickness of additional sheet of H_2O molecules.

The threshold is deeply associated with two defined hydrate structures, although its value (70%) appears to be irrational at first sight. The protonated titanate, $H_xTi_{2-x/4}\square_{x/4}O_4 \cdot H_2O$, holds one H_2O molecule in pseudocu-

(40) Jacobson, A. J.; Johnson, J. W.; Lewandowski, J. T. *Mater. Res. Bull.* **1987**, *22*, 45.

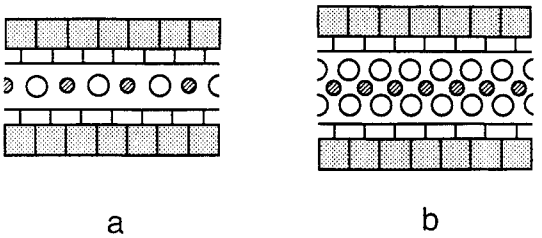

Figure 10. Plausible arrangements of interlayer cations and water molecules: (a) monolayer hydrate (<70% loading); (b) bilayer hydrate (>70%). Open and shaded circles represent water molecules and alkali-metal ions, respectively.

bic cavity enclosed by eight oxygen atoms on neighboring host layers. It is to be noted that 70% of the interlayer H_2O molecules are in the form of H_3O^+ ions, bearing exchangeable protons. The consumption of threshold amount of the exchangeable protons means that approximately half of the interlayer cavities are occupied by guest cations and the other half by H_2O (or H_3O^+).[41] It is most likely that guest cations and H_2O (or H_3O^+) molecules are arranged in an alternating way at such an interlayer composition. This hydrate structure should be stable because cations are shielded effectively by being interposed between dielectric spacers. This provides a convincing reasoning for the failure of the exchange reactions for K, Rb, and Cs ions beyond this loading. On the other hand, cations such as Li and Na are further taken up forming a bilayer cation/water cluster. Their higher hydration energy can compensate unfavorable repulsion between cations closely contacted. It is to be emphasized that the bilayer arrangement makes a cation–cation distance longer than the monolayer does, which diminishes repulsive interaction.

Similar hydrate series have been reported in layered alkali metal titanium disulfides.[42] The mode of hydration is dominated solely by polarizing power of interlayer cations, i.e., ratio of charge/radius. In $H_xTi_{2-x/4}\square_{x/4}O_4\cdot H_2O$, it is dependent on the population of cations in the interlayer as well as the nature of cations themselves.

Structure Refinements. The Rietveld refinements on some of the phases above have been carried out to get information on a precise accommodation manner of guest cations. Starting atomic coordinates for Ti and O in the host layers were taken from those for the parent titanate, $Cs_xTi_{2-x/4}\square_{x/4}O_4$.[5b] Table 3 lists refined structural parameters for Cs and K ion loaded phases which were formed at the threshold loading. The final fitted patterns for the former is depicted in Figure 11. The refinements definitely confirmed the host layers of lepidocrocite-type which arrange themselves in the body-centered relationship. The dimension of the octahedron was in a common range (see Table 4).

Figure 12 illustrates a Fourier map in the interlayer region of Cs phase, the electron density of which should be arisen from guest species. It was impossible to assign the Cs ion and the H_2O molecule independently. We first attempted to describe the hump by a virtual species of Cs/H_2O at the 2*a* position or the origin (0,0,0). The virtual species has a scattering power which is similar

(41) 0.5 ≈ 0.7 (=threshold) Å × 0.7 (=ratio of exchangeable H_3O^+ ions to the total number of cubic cavities).

(42) Schöllhorn, R. *Intercalation Chemistry*; Whittingham, M. S., Jacobson, A. J., Eds.; Academic Press: New York, 1982.

Table 3. Positional Parameters for Cs and K Ion Loaded Phases

atom	position	occupancy	*x*	*y*	*z*	B_{iso} (Å^2)
$Cs_{0.48}H_{0.22}Ti_{1.825}\square_{0.175}O_4\cdot 0.5H_2O$						
(R_{wp} = 0.075, R_p = 0.058, R_I = 0.053, R_F = 0.041)[a]						
Cs/H_2O[b]	4*i*	0.5	0.0	0.0	0.169(5)	6.8(7)
Ti	4*h*	0.9125	0.0	0.3082(6)	0.5	0.5(3)
O1	4*g*	1.0	0.0	0.219(1)	0.0	1.1(6)
O2	4*g*	1.0	0.0	0.370(2)	0.0	1.1[d]
$K_{0.48}H_{0.22}Ti_{1.825}\square_{0.175}O_4\cdot 0.7H_2O$						
(R_{wp} = 0.092, R_p = 0.067, R_I = 0.072, R_F = 0.036)[a]						
K/H_2O[c]	4*i*	0.5	0.0	0.0	0.29(1)	12.1(7)
Ti	4*h*	0.9125	0.0	0.3105(8)	0.5	0.4(4)
O1	4*g*	1.0	0.0	0.217(2)	0.0	0.8(7)
O2	4*g*	1.0	0.0	0.362(2)	0.0	0.8[d]

[a] $R_{wp} = (\Sigma w(y_o - y_c)^2/\Sigma[wy_o^2])^{1/2}$, $R_p = (\Sigma|y_o - y_c|/\Sigma y_c)$, $R_I = \Sigma|I_o - I_c|/\Sigma I_o$, $R_F = \Sigma|I_o^{1/2} - I_c^{1/2}|/\Sigma I_o^{1/2}$. [b, c] Virtual species of (0.48Cs + 0.52O) and (0.48K + 0.52O), respectively. [d] Constrained to be equal to B_{iso} for O1.

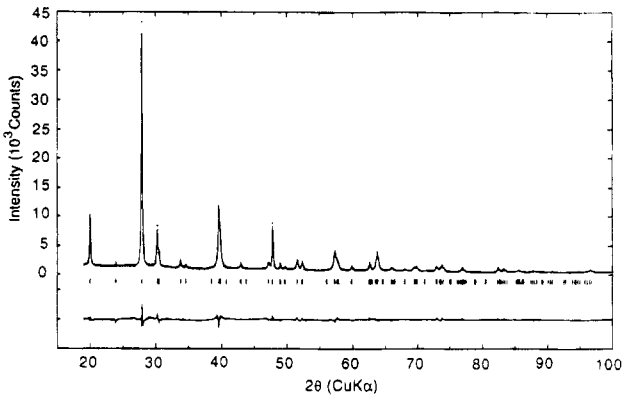

Figure 11. Observed, calculated and difference XRD profiles for the Cs phase (70% loading).

Table 4. Interatomic Distances (Å) in TiO_6 Octahedron

	Cs phase	K phase		Cs phase	K phase
Ti–O1 (×2)	1.964(6)	1.958(9)	O1–O2 (×2)	2.88(2)	2.80(3)
Ti–O2 (×2)	1.84(1)	1.75(2)	O1–O1[a] (×2)	2.9697(2)	2.9854(6)
Ti–O1[b] (×2)	2.19(2)	2.24(3)	O1–O1[b] (×4)	2.66(2)	2.69(3)
mean	1.98	1.98	mean	2.79	2.79

[a] x, y, 1 + z, [b] 1/2 − x, 1/2 − y, 1/2 + z.

to that of equally weighed Cs ion and O atom. The highly anisotropic distribution, particularly extending parallel to the *c* axis, required introduction of anisotropic temperature factors. Although significantly lowered reliability factors were obtained, a magnitude of the temperature factors, B_{eq}, was unreasonably large. Finally, splitting of Cs/H_2O into 4*i* positions, (0,0,*z*) and (0,0,$\bar{z}$), resulted in a satisfactory B_{iso} value as well as quality indexes, as listed in Table 3. The off-centered Cs ion is in a distorted cubic coordination (Cs–O: 3.15 Å × 4 and 3.59 Å × 4). Grey et al. have reported analogous splitting of interlayer Cs ions in the parent oxide $Cs_xTi_{2-x/4}\square_{x/4}O_4$.[5b]

The electron density map for K phase was more featureless and diffuse. A similar refinement procedure inevitably gave a large B_{iso} for the virtual atom of K/H_2O. The larger deviation from the origin was found for K ion. This may suggest preference of K ion for 6-fold coordination to 8-fold cubic environment.

It is manifest from these structure refinements that one interlayer virtual guests, equally weighed by cation and H_2O, is situated in every pseudocubic cavity, making a monolayer hydrate. It is reasonable to as-

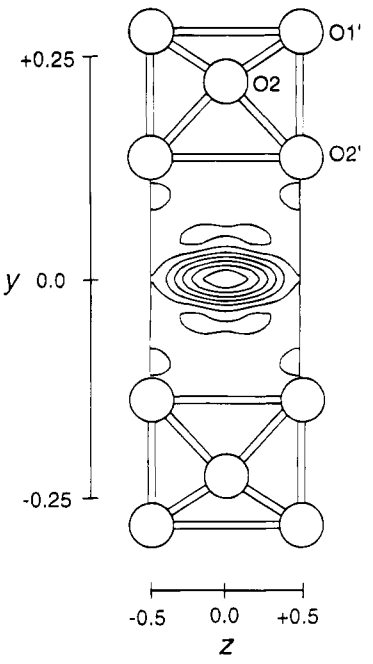

Figure 12. Electron density map in the interlayer region ($x = 0$) of the Cs phase.

Table 5.Characteristics for Protonic Layered Titanates

	ion-exchange capacity[a] (mequiv g^{-1})	interlayer spacing (Å)	charge density[b] ($Å^{-2}$)
$H_xTi_{2-x/4}\square_{x/4}O_4\cdot H_2O$ ($x = 0.7$)	4.12	9.4	1/32.2
$H_2Ti_3O_7$[c]	7.76	7.9	1/17.2
$H_2Ti_4O_9\cdot 1.2H_2O$[d]	5.57	9.1	1/22.5
$H_2Ti_5O_{11}\cdot 3H_2O$[e]	4.24	10.4	1/28.2

[a] Calculated based on the chemical formulas. [b] Calculated as $(2ac)/x$ for $H_xTi_{2-x/4}\square_{x/4}O_4\cdot H_2O$ and $(bc)/2$ for the others. [c] Reference 13c. [d] Reference 14b. [e] Reference 15.

sume that a short range ordering may develop in which cations and H_2O molecules alternate along the c axis. This ordering gives supplemental coordination for alkali metal ions and thereby contributes to stabilize the whole system.

Comparison of Various Types of Protonic Layered Titanates. Four kinds of protonic layered titanates have been reported (Table 5).[13-15] The interlayer environments change from "dry" for $H_2Ti_3O_7$ to "wet" for $H_2Ti_5O_{11}\cdot 3H_2O$ and $H_xTi_{2-x/4}\square_{x/4}O_4\cdot H_2O$, which entails swelling of interlayer separation. This tendency is roughly parallel to decrease in negative charge density of the host layers. The charge density for $H_xTi_{2-x/4}\square_{x/4}O_4\cdot H_2O$ is one of the lowest except for smectites,[43] having $\sim 1/60$ $Å^{-2}$. Most of layered materials reported so far, e.g., zirconium phosphates[39] and micas,[43] have values ranging from $1/24$ to $1/10$ $Å^{-2}$. The reciprocal of the charge density gives an estimate for a free area per negative charge, or exchangeable site. Consequently, as a rule, layered materials with low charge density facilitate incorporation of particularly bulky guests.

The low charge density for $H_xTi_{2-x/4}\square_{x/4}O_4\cdot H_2O$ may be responsible for less-defined selectivity toward alkali metal ions in comparison with the cases in $H_2Ti_4O_9\cdot 1.2H_2O$ and $H_2Ti_5O_{11}\cdot 3H_2O$. Fairly large differences in cation affinity have been observed in $H_2Ti_4O_9\cdot 1.2H_2O$ and $H_2Ti_5O_{11}\cdot 3H_2O$.[14b,15,19c,e,26a] On the other hand, $H_xTi_{2-x/4}\square_{x/4}O_4\cdot H_2O$ is less sensible as described above. The distribution coefficients and titration curves were virtually indistinguishable for K, Rb, and Cs ions. This phenomenon may be a consequence of a larger area around guest cations which results in weaker electrostatic and steric interaction between them.

Another noticeable difference is the incorporation scheme of alkali metal ions. Stepwise cation exchange has been demonstrated for $H_2Ti_4O_9\cdot 1.2H_2O$ and $H_2Ti_5O_{11}\cdot 3H_2O$.[14b,15,19c,e] A quarter- or half-portion of exchangeable protons is replaced with cations successively, producing immiscible phases of $n/4$ loading ($n = 1-4$). In contrast, the exchange processes in $H_xTi_{2-x/4}\square_{x/4}O_4\cdot H_2O$ were continuous via solid solution.

This difference is correlated with the crystal structures. The interlayer space in $H_2Ti_4O_9\cdot 1.2H_2O$ and $H_2Ti_5O_{11}\cdot 3H_2O$ consists of sectioned units which is included in the half of the unit cell. The "unit interlayer space" accommodates four exchangeable sites, the progressive substitution of which explains well the stepwise scheme, evolving intermediate phases of specific stoichiometry of $n/4$. Note that the "unit interlayer space" is chemically equivalent with each other[44] and is isolated, to some extent, from other units, which may facilitate to stabilize the intermediates. On the other hand, $H_xTi_{2-x/4}\square_{x/4}O_4\cdot H_2O$ is characterized by its rather uniform interlayer galleries. The minimum unit corresponds to the pseudocubic cavity. This structural feature brings about continuous incorporation. The "unit interlayer space" is one of the most dominant structural characteristics which governs intercalation behavior in the series of the protonic layered titanates.

CM950014H

(43) Brindley, G. W.; Brown, G. *Crystal Structures of Clay Minerals and Their X-Ray Identification*; Mineralogical Society: London, 1980.

(44) The "unit interlayer space" is not structurally equivalent, having two different levels along the b axis.